Kinetics of Surface-Induced Dissociation of $N(CH_3)_4^+$ and $N(CD_3)_4^+$ Using Silicon Nanoparticle Assisted Laser Desorption/Ionization and Laser Desorption/Ionization

Sung Hwan Yoon, Chaminda M. Gamage,* Kent J. Gillig,† and Vicki H. Wysocki

Department of Chemistry and Biochemistry, University of Arizona, Tucson, Arizona, USA

The implementation of surface-induced dissociation (SID) to study the fast dissociation kinetics (sub-microsecond dissociation) of peptides in a MALDI TOF instrument has been reported previously. Silicon nanoparticle assisted laser desorption/ionization (SPALDI) now allows the study of small molecule dissociation kinetics for ions formed with low initial source internal energy and without MALDI matrix interference. The dissociation kinetics of $N(CH_3)_4^+$ and $N(CD_3)_4^+$ were chosen for investigation because the dissociation mechanisms of $N(CH_3)_4^+$ have been studied extensively, providing well-characterized systems to investigate by collision with a surface. With changes in laboratory collision energy, changes in fragmentation timescale and dominant fragment ions were observed, verifying that these ions dissociate via unimolecular decay. At lower collision energies, methyl radical (CH_3) loss with a sub-microsecond dissociation rate is dominant, but consecutive H loss after CH_3 loss becomes dominant at higher collision energies. These observations are consistent with the known dissociation pathways. The dissociation rate of CH_3 loss from $N(CH_3)_4^+$ formed by SPALDI and dissociated by an SID lab collision energy of 15 eV corresponds to log k = 8.1, a value achieved by laser desorption ionization (LDI) and SID at 5 eV. The results obtained with SPALDI SID and LDI SID confirm that (1) the dissociation follows unimolecular decay as predicted by RRKM calculations; (2) the SPALDI process deposits less initial energy than LDI, which has advantages for kinetics studies; and (3) fluorinated self-assembled monolayers convert about 18% of laboratory collision energy into internal energy. SID TOF experiments combined with SPALDI and peak shape analysis enable the measurement of dissociation rates for fast dissociation of small molecules. (J Am Soc Mass Spectrom 2009, 20, 957–964) © 2009 Published by Elsevier Inc. on behalf of American Society for Mass Spectrometry

Details of the dissociation mechanisms and dissociation rates of ions under given energy-transfer conditions remain a subject of intense study. Tandem mass spectrometry (MS/MS), with a wide range of ion activation methods, has been used to investigate dissociation mechanisms [1–8]. Collision-induced dissociation (CID) is the most common activation method applied in MS/MS. An alternative technique to CID, surface-induced dissociation (SID) [8] has been successfully used for ion fragmentation studies of small molecules [9–14], peptides [15–23], and large molecules and macromolecular assemblies such as proteins and protein/protein complexes [24–26]. Other aspects of SID have been reviewed elsewhere [27–29]. Compared to CID, SID has several advantages. Most notably, SID is a single-collision process with a defined impact plane and arrival time, a very fast activation time [30], and high kinetic to internal energy conversion efficiency. Rice–Ramsperger–Kassel–Marcus (RRKM) modeling has successfully explained unimolecular decay processes by SID [18–20]. Dynamics simulations have also been carried out to investigate ion-surface collisions [31, 32].

Matrix-assisted laser desorption/ionization surface-induced dissociation time-of-flight (MALDI SID TOF) spectra of small peptides, such as des-R^1-bradykinin and des-R^9-bradykinin, were reported previously [21].

Address reprints requests to Dr. Vicki H. Wysocki, University of Arizona, Department of Chemistry and Biochemistry, 1306 E. University Blvd., Tucson, AZ 85721-0041. E-mail: vwysocki@email.arizona.edu

* Present address: Masstech Inc., 6992 Columbia Gateway Drive, Columbia, MD 21046, USA.

† Present address: Department of Chemistry, Texas A&M University, College Station, TX 77842, USA.

1044-0305/09/$32.00
doi:10.1016/j.jasms.2009.03.001

Published online March 6, 2009
Received January 5, 2009
Revised March 1, 2009
Accepted March 2, 2009

Calculations of average fragmentation times indicate a ten to hundreds of nanoseconds timescale, suggesting the involvement of a fast unimolecular decay process. The rate of these decay processes depends on the collision energy. As the collision energy is increased, the fragmentation efficiency of the precursor ion increases. This is accompanied by an increase in the intensity and the number of fragment ions as the collision energy is increased. A study of the different fragmentation timescales and patterns associated with the varying collision energies suggests that the predominant fragmentation processes for MALDI SID TOF of des-R^1 and des-R^9 bradykinin are fast unimolecular decay [21] rather than the alternative pathway of shattering [19].

Although our modified MALDI TOF instrument was successfully combined with SID to explore fast dissociation processes, the study of small molecules was complicated by MALDI matrix interference. Recently, the Wysocki group has reported ionization via silicon nanoparticle assisted laser desorption/ionization (SPALDI) [33–35]. SPALDI has been successful in generating molecular ions from analytes ranging in size from small organics such as $N(CH_3)_4^+$ to peptides without matrix assistance and with much lower laser fluence than MALDI or laser desorption/ionization (LDI).

$N(CH_3)_4^+$ has received much attention because of its characteristic dissociation patterns. Dissociation kinetics of $N(CH_3)_4^+$ have been studied by different methods such as SID in a triple quadruple instrument [11], CID in a sector instrument [36], and by RRKM calculations [37]. RRKM results show that CH_4 loss is dominant at very low internal energies, but that the rate of CH_3 elimination increases faster than that of CH_4 loss with increasing energy. CH_4 elimination takes place through two reaction pathways: a direct elimination by rearrangement of $N(CH_3)_4^+$ and consecutive losses of CH_3 and H. Experimental results show that the increase of CH_4 loss at high energies occurs through the consecutive reaction rather than by rearrangement. Detailed experiments and calculations found that CH_3 loss is more dominant above 400 kJ/mol internal energy than CH_4 elimination and at higher internal energies CH_3 loss is always faster than CH_4 elimination by rearrangement. $N(CD_3)_4^+$ was shown to have the same reaction paths as those of $N(CH_3)_4^+$ [36]. In the present study, $N(CH_3)_4^+$ and $N(CD_3)_4^+$ were selected as model systems for SPALDI SID TOF experiments with peak shape analysis. The molecular ions are generated by SPALDI or LDI and activated by a single collision with a surface and the peak shapes of resulting fragment ions are analyzed to interpret fragmentation kinetics. The peak shape analysis model is implemented by a convolution of the first-order unimolecular dissociation process with the arrival time distribution at the surface, resulting in an estimated rate for CH_3 (CD_3) loss and an evaluation of relative differences in extents of source activation by SPALDI and LDI.

Experimental

A MALDI TOF instrument (Proflex, Bruker Daltonics, Billerica, MA, USA) was modified by introducing an SID setup as reported previously and presented in Figure 1 [21]. Briefly, a flange-mounted surface assembly was introduced into the time-of-flight tube behind the reflectron ion optics. The surface assembly consists of a collision target with a brass holder and a Ni grid (20-line mesh; BMC Industries Inc., St Paul, MN, USA), which were electrically isolated from each other by a 5-mm-thick Macor spacer. The extraction grid, a brass holder, Macor spacers, and a collision target were mounted on a custom-built assembly consisting of a z-movable stage (model BLM-2751; MDC, Hayward, CA, USA) combined with a set of hinges, allowing variation of the angle between the target surface and the plane parallel to the last reflectron electrode. The collision energy for singly charged ions is defined by the voltage difference between the target plate of the source and the collision target. The delayed extraction scheme previously used in the SID ion extraction region [21] was not used in the present experiments because uniform and consistent extraction electric fields are desired for the peak shape analysis model. The surface setup is interchangeable with a floating detector (Bipolar MCP, Burle, Lancaster, PA, USA), which has a similar dimension to the SID setup. The detector has the capability of floating at similar electric potential as that of the collision target, so the voltage difference between the floating detector and the surface is the same as the collision energy. Changing voltages of the floating detector enables the measurement of the arrival time distribution of the ion packet corresponding to different collision energies.

The peak shape analysis model assumes a first-order unimolecular decay process for parent ion dissociation, as shown in Figure 2. The fragment ion intensity increases exponentially as the parent ion intensity decreases exponentially. This exponential curve (which

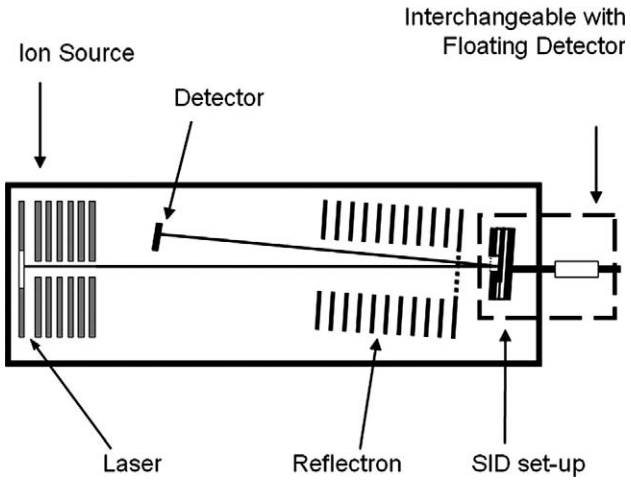

Figure 1. Schematic diagram of MALDI SID TOF modified from Bruker Proflex.

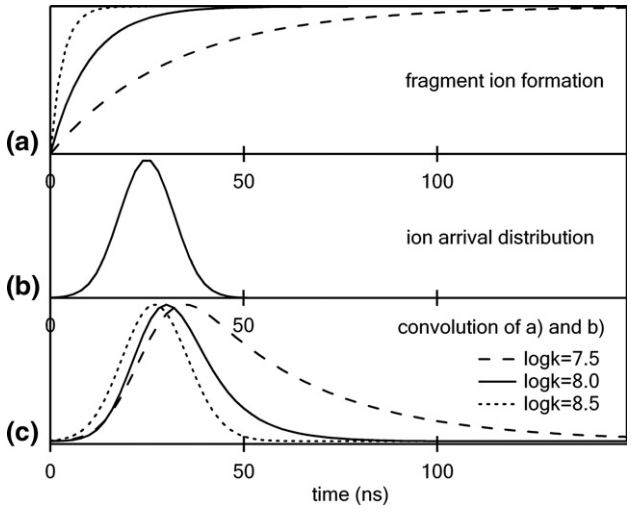

Figure 2. Peak shape analysis model (**a**) fragment ion formation at log k values of 7.5, 8.0, 8.5; (**b**) incoming ion arrival distribution at the surface; (**c**) convolution of (**a**) and (**b**).

indicates the fraction of precursor converted to fragment at a given time after activation) is convoluted with the arrival time distribution of the ion packet at the surface (a distribution that is experimentally obtained by using the floating detector). For the curves shown in Figure 2, log k values of 7.5, 8.0, and 8.5 are illustrated for the parent ion decay and the mean value of 25 ns and standard deviation value of 7 are used for the arrival ion distribution, values similar to actual experimental results. The kinetic energy distribution of the ion packet arriving at the surface is not known accurately and needs to be studied further, but that is outside of the scope of the present work. We also assumed that there is no significant kinetic energy release associated with the losses under investigation [36]. Only the surface arrival time distribution is considered at this point. The dissociation rate inversely affects the peak width as shown in Figure 2: as dissociation rates increase, the convoluted model peak becomes narrower (log k = 8.5). Conversely, slower reactions cause peak broadening (log k = 7.5). This calculated convoluted peak is compared with the experimental results to estimate the average dissociation rate of a specific dissociation pathway. For the direct CH_3 loss and consecutive H loss of $N(CH_3)_4^+$, a first-order unimolecular decay model with consecutive reactions was applied for convolution [38]. The fragmentation pathway considered and the corresponding rate expressions are shown as eqs 1–3. A_1 represents for the precursor ion, $N(CH_3)_4^+$, A_2 is the fragment ion corresponding to CH_3 loss, and A_3 is the product formed after consecutively losing CH_3 and H. Equations 2 and 3 were convoluted with the ion arrival distribution and various k_1 and k_2 were applied to establish the best peak fit.

$$A_1 \xrightarrow{k_1} A_2 \xrightarrow{k_2} A_3 \quad (1)$$

$$[A_2] = \frac{[A_1]_0 k_1}{k_2 - k_1}\left(e^{-k1t} - e^{-k2t}\right) \quad (2)$$

$$[A_3] = [A_1]_0\left(1 - \frac{k_2}{k_2 - k_1}e^{-k1t} + \frac{k_1}{k_2 - k_1}e^{-k2t}\right) \quad (3)$$

A chemically modified gold surface was used in the SID experiments. Glass surfaces coated with a 50-Å layer of titanium followed by a 1000-Å layer of gold (Evaporated Metal Films Corp., Ithaca, NY, USA) were used as substrates for preparing the SID collision targets. The Au-coated slide was UV cleaned for 15 min (Boekel UV cleaner model 135500; Boekel Industries, Inc., Feasterville, PA, USA), rinsed with ethanol, and immersed in a 1 mM ethanolic solution of 2-(perfluorodecyl)ethanethiol [fluorinated self-assembled monolayer (FSAM), $CF_3(CF_2)_9(CH_2)_2SH$, C12F10] for 24 h. After 24 h, the surface was immersed in ethanol and cleaned in an ultrasonic bath for 1 min. The sonication was repeated for a total of six cycles using fresh ethanol each time. Hydrogenated SAM surfaces were prepared in the same manner, using hexadecanethiol [HSAM, $CH_3(CH_2)_{15}SH$, C16F0] instead of C12F10. The thiols used for SAM formation on the SID collision target were synthesized by the Chemical Synthesis Facility of the Department of Chemistry and Biochemistry, University of Arizona. The surface preparation technique is further explained elsewhere [39]. $N(CH_3)_4^+$ was purchased as the hydroxide from Sigma–Aldrich (St. Louis, MO, USA) and dissolved in 25% wt methanol. $N(CD_3)_4^+$ was purchased from Cambridge Isotope Laboratories Inc. (Andover, MA, USA) as the chloride.

SPALDI and LDI were used for the desorption/ionization methods. SPALDI has been introduced by the Wysocki research group and the details were reported elsewhere [33]. The 30-nm silicon particles purchased from Meliorum Technologies Inc. (Rochester, NY, USA) were oxidized with 10% HNO_3 by 30-min sonication and dried thoroughly in a vacuum concentrator. The oxidized particles were derivatized with (heptadecafluoro-1,1,2,2-tetrahydrodecyl)dimethylchlorosilane (C10) for 10 h at 90 °C, rinsed with isopropanol, and stored in perfluorohexane (Fluka, St. Louis, MO, USA). $N(CH_3)_4^+$ or $N(CD_3)_4^+$ at a concentration of 100 pmol/μL was mixed with derivatized silicon particles in a 1:1 ratio of isopropanol/H_2O and was deposited on a commercial MALDI plate. For LDI, $N(CH_3)_4^+$ or $N(CD_3)_4^+$, at a concentration of 100 pmol/μL, was deposited directly on the MALDI plate. For SPALDI and LDI, samples were directly irradiated by the N_2 laser (VSL337i, Laser Science Inc., Newton, MA, USA), whose maximum energy is 150 μJ, operated at a repetition rate of 3 Hz for both ionization methods. For each spectrum shown here, spectra from at least 200–300 laser shots were averaged to increase signal to noise ratios.

Results and Discussion

Studies were performed on the MALDI SID TOF instrument to determine compatibility of $N(CH_3)_4^+$ with LDI and SPALDI. In this MALDI SID TOF instrument, LDI of $N(CH_3)_4^+$ without silicon powder requires 50–60% of the total laser intensity (50–40% attenuation) and MALDI of small peptides such as YGGFLR and bradykinin require about 65–80% laser intensity (35–20% attenuation) to generate precursor ions. By contrast, SPALDI of $N(CH_3)_4^+$ requires only 5% laser intensity (95% attenuation), which is very low compared to that of LDI and MALDI. After the success of the initial experiments, $N(CH_3)_4^+$ generated by SPALDI was subsequently subjected to SID. To obtain strong fragment ion signals for peak shape analysis, intense parent ion beams are required before the surface collision, so 25% laser intensity (75% attenuation) was used for the SPALDI experiments. Before dissociation of the parent ion, it is important to confirm that only $N(CH_3)_4^+$ is desorbed from the source. Voltages higher than 9 kV, which is the source acceleration voltage, were applied to the surface to turn incoming ions to avoid hitting the surface. In this experiment only the precursor ion was observed, as shown in Figure 3a, confirming the absence of other ions that might have been generated at the source. LDI of $N(CH_3)_4^+$ showed the same result (data not shown). After this confirmation, surface voltages were lowered to cause collisions between incoming ions and the surface.

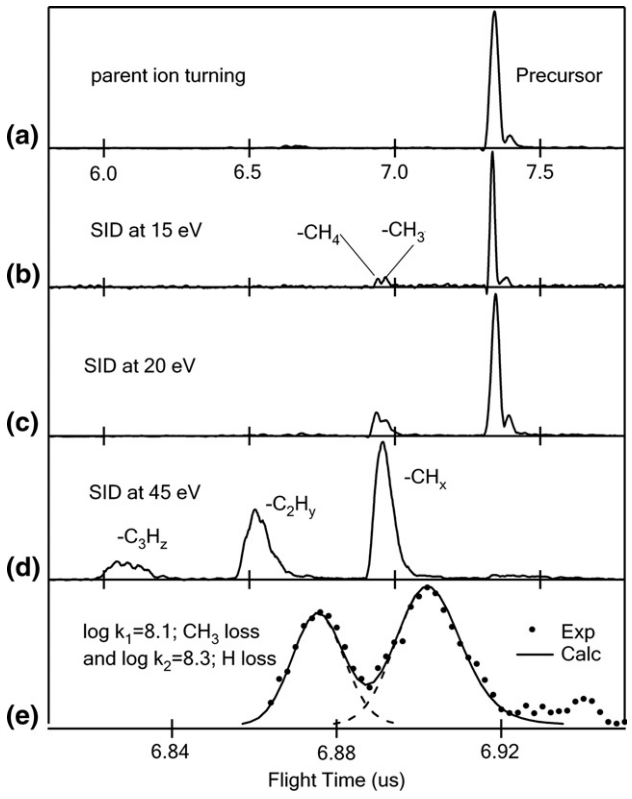

Figure 3. SPALDI SID TOF of $N(CH_3)_4^+$ on fluorinated SAM (**a**) parent ion turning; (**b**) SID at 15 eV; (**c**) SID at 20 eV; (**d**) SID at 45 eV; (**e**) best peak fit of (**b**) corresponds to log k_1 = 8.1 and log k_2 = 8.3.

SPALDI SID TOF of $N(CH_3)_4^+$, which is shown in Figure 3b–d, yielded different dissociation pathways as a function of collision energy. With a change in laboratory collision energy of the ions there was a change in the internal vibrational energy deposition, which led to observation of variations in the fragmentation timescale and dominant fragment ions. The fact that the dissociation of $N(CH_3)_4^+$ varies as a function of internal energy demonstrates that the dissociation is unimolecular and consistent with previously reported data [11, 36]. Figure 3b shows the first fragmentation channels are CH_3 loss and CH_4 loss. The CH_4 loss might be from rearrangement dissociation of CH_4 or CH_3 cleavage followed by H loss. Reducing collision energies to less than 15 eV generated CH_3 loss predominantly in this given observation time window, but the fragment ions at even lower collision energies are difficult to measure because of kinetic shifts. If a low enough collision energy was given to produce an ion internal energy of less than 400 kJ/mol, and a longer observation time window was provided, CH_4 loss should have been detected predominantly according to previous studies [37]. The spectrum shown in Figure 3c was observed at 5 eV higher SID collision energy than that in Figure 3b, and shows a preference of overall [CH_3 + H] loss over CH_3 loss. Figure 3d at 45 eV SID energy shows that the parent ion does not survive and multiple dissociation pathways are observed at this collision energy. Figure 3 shows that at lower collision energy CH_3 loss is dominant, but additional H loss after CH_3 loss becomes more dominant at higher collision energy. This overall [CH_3 + H] loss occurs at high internal energy with fast dissociation time. As previously mentioned, CH_4 loss by rearrangement occurs at low internal energy with very long dissociation time frame, so CH_4 rearrangement is not involved in this case. The signal-to-noise (S/N) ratio and resolution are not as high as those of a previously reported experiment [21]. Although delayed extraction would improve the S/N ratio and resolution, delayed extraction in the surface region was not used, to keep electric fields static and uniform inside the instrument. This is important to simulate the dissociation and apply peak shape analysis without added complexity.

Figure 4 shows the SID energy resolved MS/MS data indicating the branching ratio of each reaction channel shown in Figure 3 with the ratios calculated based on peak areas. The areas of each peak representing individual fragmentation channels were normalized at each collision energy and the relative areas of fragmentation channels were compared. CH_x is the sum of both CH_3 and [CH_3 + H] losses because, at higher collision energies, the CH_3 loss product continues to dissociate, leading to a net loss of CH_4 and the resolution of the experiment is not sufficient to separate these peaks well at higher collision energies. At even higher collision energies, the precursor ion loses multiple carbon units

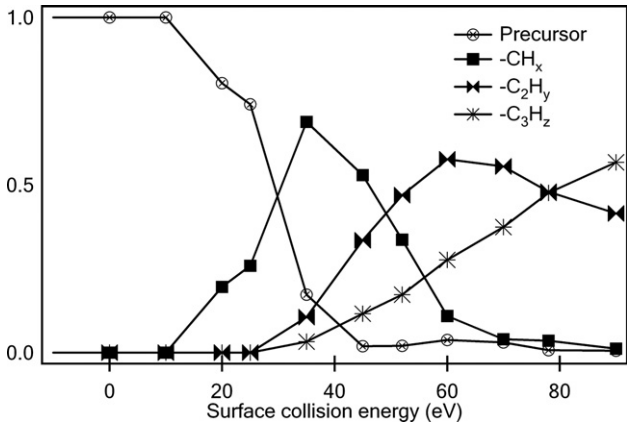

Figure 4. Energy resolved MS/MS curve of $N(CH_3)_4^+$ based on Figure 3.

and C_2H_y and C_3H_z are used to describe these peaks corresponding to further fragmentation. The peaks are not identified by numbers of hydrogens. Consistent with Figure 3, as the collision energy increases more dissociation occurs and the lower *m/z* fragments become dominant. Figure 4 clearly shows that fragmentation patterns vary significantly and systematically with different collision energies, which is a typical characteristic of unimolecular decay.

Peak shape analysis was carried out for the CH_3 and subsequent H losses at the collision energy of 15 eV and the result is shown in Figure 3e. At 15 eV, the surface arrival distribution obtained by replacing the surface with the floating detector was 25 ns at full width of half-maximum (FWHM). A Gaussian distribution with mean value of 25 ns and standard deviation value of 7 was used for the surface arrival distribution. Similar mean and standard deviation values, measured by the floating detector for different collision energies, were used for later peak fittings. Because the formal CH_4 loss is really two consecutive reactions involving CH_3 and H losses, rate expressions for first-order consecutive unimolecular dissociation were considered. Plots with different dissociation rate constants k were used for convolution with the arrival time distribution to fit to the experimental results and log k_1 = 8.1 for CH_3 loss and log k_2 = 8.3 for subsequent H loss provided the best fit. The fastest dissociation reaction that the instrument can measure is 2 ns because of the maximum rate of the digitizer, which corresponds to log k = 8.7 and the slowest reaction measurable for $N(CH_3)_4^+$ is about 170 ns, corresponding to a log k of 6.8. The obtained match of log k = 8.1 confirms that the CH_3 loss takes place within the time window of the SID TOF instrument and the peak shape analysis model gives a reasonable dissociation rate.

The obtained log k = 8.1 can be compared with the RRKM curve from the work of Hudson et al. [37]. At a decay rate of log k = 8.1, the ion internal energy is roughly 570 kJ/mol which is about 5.8 eV. This 5.8 eV includes the initial energy deposition from the ionization process and the translational energy (T) to internal vibrational energy (V) conversion during the surface collision. If the initial energy deposition during ionization is neglected—a poor assumption—one would calculate that 41% of the translational energy is converted to the internal vibrational energy for a 15 eV collision. The energy conversion of fluorinated SAM surfaces has been reported to reach about 20–30%, suggesting that ionization probably contributes some initial internal energy into the ion packet [40, 41]. The initial energy deposition of SPALDI has been estimated as about 2.7–3.6 eV for substituted benzylpyridinium ions [35]. Considering the midpoint of this range of initial energies, it can be concluded that about 18% of translational energy was converted into internal vibrational energy on a fluorocarbon surface, which is consistent with previous results. A source energy of around 3 eV is reasonable, given that CH_3 loss from $N(CH_3)_4^+$ has an appearance energy about 3.2–3.4 eV [36, 37] and the acceleration field in the ion source defines the source dissociation time (~1 μs) such that 5 eV would be required to see source fragmentation and none was detected (see Figure 3a) [37].

As mentioned earlier, SPALDI requires less laser intensity than LDI [34, 35], which can lead to lower internal energy deposition during the ionization process. If an ion has high internal energy before SID, only a small amount of additional energy is required to overcome the energy barrier for dissociation. To investigate this effect further, LDI SID was used to compare with SPALDI SID and the results are shown in Figure 5. A 5 eV collision for LDI SID ions gives a similar SID spectrum to a 15 eV collision for SPALDI SID and 10 eV

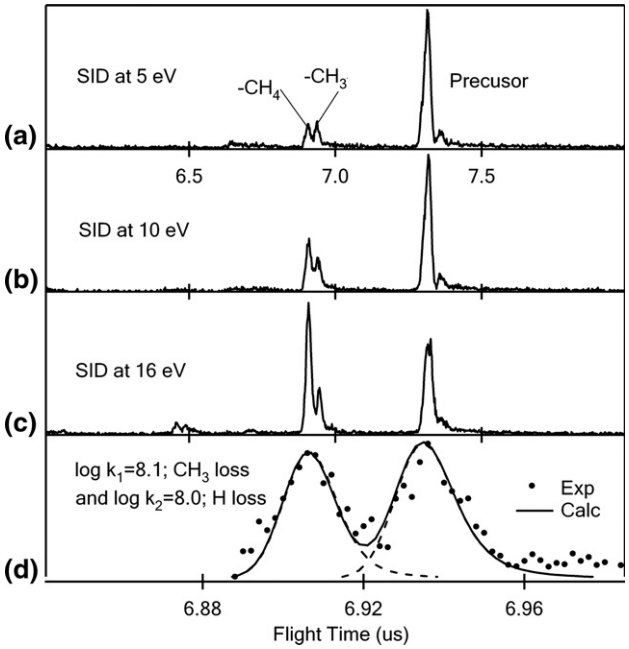

Figure 5. LDI SID TOF of $N(CH_3)_4^+$ on fluorinated SAM (**a**) SID at 5 eV; (**b**) SID at 10 eV; (**c**) SID at 16 eV; (**d**) best peak fit of (**a**) corresponds to log k_1 = 8.1 and log k_2 = 8.0.

for LDI SID compares well to 20 eV for SPALDI SID. A CH_3 loss at 5 eV of LDI SID gives log k = 8.1 with a consecutive H loss with a log k = 8.0 by peak shape analysis. The peak fit is shown in Figure 5d and is similar to the result for 15 eV SPALDI SID shown in Figure 3e. As shown in Figure 5, LDI SID needed about 10 eV less collision energy to observe the same dissociation phenomenon, which verifies that LDI-produced ions are relatively "hotter" and SPALDI is a "colder" ionization process. Because LDI deposits more internal energy to the ion, less collision energy is required to fragment the ion within the same time window. Earlier results by the Wysocki group confirmed that SPALDI deposits less internal energy than MALDI as well [33]. Therefore, the use of SPALDI for kinetics studies is promising.

Dissociation kinetic studies with SPALDI and LDI can be performed with other molecules to further verify the applicability of the SID TOF instrument. It was previously reported that $N(CD_3)_4^+$ undergoes dissociation pathways that parallel those of $N(CH_3)_4^+$ [36]. Deuterated $N(CH_3)_4^+$ can be used to obtain larger peak separations because deuterium is heavier than hydrogen, making the flight time difference between CD_3 and [CD_3 + D] greater. The SID results for $N(CD_3)_4^+$ formed by LDI and SPALDI are shown in Figures 6 and 7, respectively. Dissociation of deuterated molecules requires higher energy than hydrogenated molecules because of the kinetic isotope effect. Both LDI (Figure 6) and SPALDI SID (Figure 7) spectra showed that $N(CD_3)_4^+$ needs higher collision energies to reach the same extents of dissociation as $N(CH_3)_4^+$. Again, ions

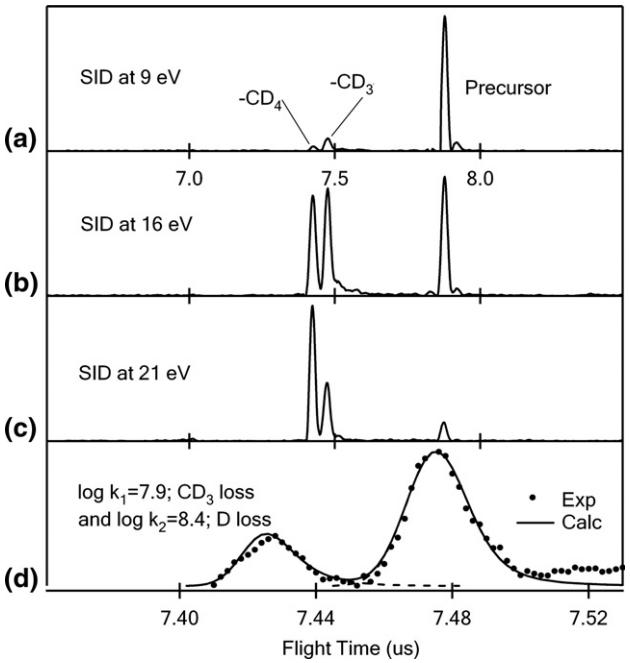

Figure 6. LDI SID TOF of $N(CD_3)_4^+$ on fluorinated SAM (**a**) SID at 9 eV; (**b**) SID at 16 eV; (**c**) SID at 21 eV; (**d**) best peak fit of (**a**) corresponds to log k_1 = 7.9 and log k_2 = 8.4.

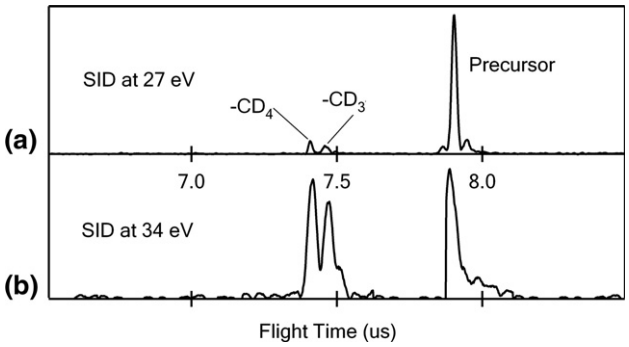

Figure 7. SPALDI SID TOF of $N(CD_3)_4^+$ on fluorinated SAM (**a**) SID at 27 eV; (**b**) SID at 34 eV.

formed by SPALDI need higher SID energies than those formed by LDI to show the similar extents of dissociation for the same compound. The baseline is fully resolved and a log k value of 7.9 was obtained for CD_3 loss and 8.4 for consecutive D loss at 9 eV SID with LDI as shown in Figure 6d.

The peak shape modeling can also be applied to explore the influence of surface type on dissociation rate. Reactive ion scattering spectrometry (RISS) has been applied to study a variety of surfaces [42]. Hydrogenated surfaces are known to have lower energy conversion efficiency than that of fluorinated surfaces [41]. LDI SID TOF of $N(CD_3)_4^+$ for collision with a hydrogenated surface is shown in Figure 8; the best-fit dissociation rate for CD_3 loss was log k_1 = 7.8 and subsequent D loss was log k_2 = 8.3. Compared with Figure 6d, to have similar extents of dissociation and log k values, the hydrogenated surface requires higher SID collision energy, which confirms that hydrogenated surfaces have lower energy conversion efficiency than that of fluorinated surfaces. However, the surface studies using this approach are still at an early stage and further studies are required for various surface types.

Conclusions

The feasibility of surface-induced activation in a TOF instrument was reported previously. In this work, an

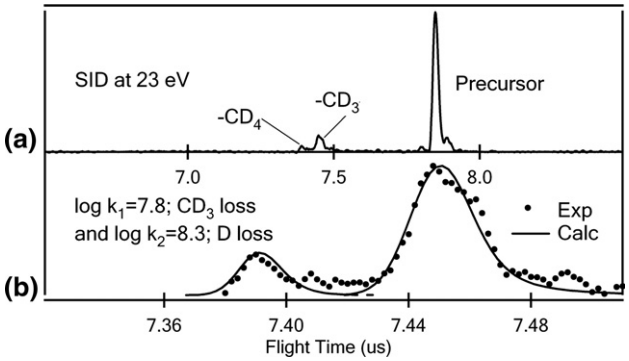

Figure 8. LDI SID TOF of $N(CD_3)_4^+$ on hydrogenated SAM (**a**) SID at 23 eV; (**b**) best peak fit of (**a**) corresponds to log k_1 = 7.8 and log k_2 = 8.3.

SID TOF system was used to study the dissociation kinetics of $N(CH_3)_4^+$ and $N(CD_3)_4^+$. Fast dissociation channels of $N(CH_3)_4^+$ and $N(CD_3)_4^+$ were investigated with a peak shape analysis model. Although this experiment had lower resolution than that of previously reported experiments because of the intentional lack of a delayed extraction pulse at the surface, the fragment ion peaks were resolved enough to apply the peak shape model for CH_3 (CD_3) loss and subsequent H (D) loss at low collision energies. Dissociation patterns followed previously reported trends for unimolecular dissociation and fast dissociation of CH_3 (CD_3) within hundreds of nanoseconds was successfully observed within the time window of the SID setup. The obtained dissociation rate was reasonably well matched with reported RRKM calculations considering initial ion source energy deposition and T→V energy conversion efficiency of the FSAM surface. SPALDI gives less internal energy deposition than that of MALDI and LDI, which is an advantage for experimentally determining more accurate dissociation rates and energy transfer from the surface. Additionally, this research confirmed differences in energy deposition for different surface types. In the future, kinetics of dissociation of larger molecules such as peptides will be investigated by this SID approach.

Acknowledgments

The authors acknowledge Bruker Daltonics for the donation of a Proflex MALDI TOF MS and Dr. Mel Park and Doug Roderick for helpful discussions. This research was supported by the National Science Foundation under Grant CHE-0416388 awarded to Dr. Vicki Wysocki. The authors thank Dr. Ronald Wysocki for the synthesis of 2-(perfluorodecyl)ethanethiol and hexadecanethiol and Dr. Arpad Somogyi for helpful discussions.

References

1. Gauthier, J. W.; Trautman, T. R.; Jacobson, D. B. Sustained Off-Resonance Irradiation for Collision-Activated Dissociation Involving Fourier-Transform Mass-Spectrometry–Collision-Activated Dissociation Technique That Emulates Infrared Multiphoton Dissociation. *Anal. Chim. Acta* **1991,** *246,* 211–225.
2. Woodin, R. L.; Bomse, D. S.; Beauchamp, J. L. Multi-Photon Dissociation of Molecules with Low-Power Continuous Wave Infrared-Laser Radiation. *J. Am. Chem. Soc.* **1978,** *100,* 3248–3250.
3. Little, D. P.; Speir, J. P.; Senko, M. W.; O'Connor, P. B.; McLafferty, F. W. Infrared Multiphoton Dissociation of Large Multiply-Charged Ions for Biomolecule Sequencing. *Anal. Chem.* **1994,** *66,* 2809–2815.
4. Price, W. D.; Schnier, P. D.; Williams, E. R. Tandem Mass Spectrometry of Large Biomolecule Ions by Blackbody Infrared Radiative Dissociation. *Anal. Chem.* **1996,** *68,* 859–866.
5. Zubarev, R. A.; Kelleher, N. L.; McLafferty, F. W. Electron Capture Dissociation of Multiply Charged Protein Cations. A Nonergodic Process. *J. Am. Chem. Soc.* **1998,** *120,* 3265–3266.
6. Syka, J. E. P.; Coon, J. J.; Schroeder, M. J.; Shabanowitz, J.; Hunt, D. F. Peptide and Protein Sequence Analysis by Electron Transfer Dissociation Mass Spectrometry. *Proc. Natl. Acad. Sci. U. S. A.* **2004,** *101,* 9528–9533.
7. McLafferty, F. W. *Tandem Mass Spectrometry*. Wiley: New York, 1983.
8. Cooks, R. G.; Terwilliger, D. T.; Ast, T.; Beynon, J. H.; Keough, T. Surface Modified Mass-Spectrometry. *J. Am. Chem. Soc.* **1975,** *97,* 1583–1585.
9. Wysocki, V. H.; Kenttamaa, H. I.; Cooks, R. G. Internal Energy-Distributions of Isolated Ions after Activation by Various Methods. *Int. J. Mass Spectrom. Ion Processes* **1987,** *75,* 181–208.
10. Ijames, C. F.; Wilkins, C. L. Surface-Induced Dissociation by Fourier-Transform Mass-Spectrometry. *Anal. Chem.* **1990,** *62,* 1295–1299.
11. Wysocki, V. H.; Ding, J. M.; Jones, J. L.; Callahan, J. H.; King, F. L. Surface-Induced Dissociation in Tandem Quadrupole Mass Spectrometers: A Comparison of Three Designs. *J. Am. Soc. Mass Spectrom.* **1992,** *3,* 27–32.
12. Burroughs, J. A.; Wainhaus, S. B.; Hanley, L. Impulsive Excitation of $Cr(Co)_6^+$ During Surface-Induced Dissociation at Organic Monolayers. *J. Phys. Chem.* **1994,** *98,* 10913–10919.
13. Worgotter, R.; Kubista, J.; Zabka, J.; Dolejsek, Z.; Mark, T. D.; Herman, Z. Surface-Induced Reactions and Decomposition of the Benzene Molecular Ion $C_6H_6^+$: Product Ion Intensities, Angular and Translational Energy Distributions. *Int. J. Mass Spectrom.* **1998,** *174,* 53–62.
14. Laskin, J.; Denisov, E.; Futrell, J. A Comparative Study of Collision-Induced and Surface-Induced Dissociation. 1. Fragmentation of Protonated Dialanine. *J. Am. Chem. Soc.* **2000,** *122,* 9703–9714.
15. Williams, E. R.; Henry, K. D.; McLafferty, F. W.; Shabanowitz, J.; Hunt, D. F. Surface-Induced Dissociation of Peptide Ions in Fourier-Transform Mass-Spectrometry. *J. Am. Soc. Mass Spectrom.* **1990,** *1,* 413–416.
16. Dongre, A. R.; Somogyi, A.; Wysocki, V. H. Surface-Induced Dissociation: An Effective Tool to Probe Structure, Energetics and Fragmentation Mechanisms of Protonated Peptides. *J. Mass Spectrom.* **1996,** *31,* 339–350.
17. Stone, E.; Gillig, K. J.; Ruotolo, B.; Fuhrer, K.; Gonin, M.; Schultz, A.; Russell, D. H. Surface-Induced Dissociation on a Maldi-Ion Mobility-Orthogonal Time-of-Flight Mass Spectrometer: Sequencing Peptides from an "In-Solution" Protein Digest. *Anal. Chem.* **2001,** *73,* 2233–2238.
18. Laskin, J.; Denisov, E.; Futrell, J. H. Fragmentation Energetics of Small Peptides from Multiple-Collision Activation and Surface-Induced Dissociation in FT-ICR MS. *Int. J. Mass Spectrom.* **2002,** *219,* 189–201.
19. Laskin, J.; Bailey, T. H.; Futrell, J. H. Shattering of Peptide Ions on Self-Assembled Monolayer Surfaces. *J. Am. Chem. Soc.* **2003,** *125,* 1625–1632.
20. Laskin, J. Energetics and Dynamics of Peptide Fragmentation from Multiple-Collision Activation and Surface-Induced Dissociation Studies. *Eur. J. Mass Spectrom.* **2004,** *10,* 259–267.
21. Gamage, C. M.; Fernandez, F. M.; Kuppannan, K.; Wysocki, V. H. Submicrosecond Surface-Induced Dissociation of Peptide Ions in a MALDI TOF MS. *Anal. Chem.* **2004,** *76,* 5080–5091.
22. Fernandez, F. M.; Wysocki, V. H.; Futrell, J. H.; Laskin, J. Protein Identification via Surface-Induced Dissociation in an FT-ICR Mass Spectrometer and a Patchwork Sequencing Approach. *J. Am. Soc. Mass Spectrom.* **2006,** *17,* 700–709.
23. Yoon, O. K.; Robbins, M. D.; Zuleta, I. A.; Barbula, G. K.; Zare, R. N. Continuous Time-of-Flight Ion Imaging: Application to Fragmentation. *Anal. Chem.* **2008,** *80,* 8299–8307.
24. Chorush, R. A.; Little, D. P.; Beu, S. C.; Wood, T. D.; McLafferty, F. W. Surface-Induced Dissociation of Multiply Protonated Proteins. *Anal. Chem.* **1995,** *67,* 1042–1046.
25. Jones, C. M.; Beardsley, R. L.; Galhena, A. S.; Dagan, S.; Cheng, G. L.; Wysocki, V. H. Symmetrical Gas-Phase Dissociation of Noncovalent Protein Complexes Via Surface Collisions. *J. Am. Chem. Soc.* **2006,** *128,* 15044–15045.
26. Galhena, A. S.; Dagan, S.; Jones, C. M.; Beardsley, R. L.; Wysocki, V. N. Surface-Induced Dissociation of Peptides and Protein Complexes in a Quadrupole/Time-of-Flight Mass Spectrometer. *Anal. Chem.* **2008,** *80,* 1425–1436.
27. Grill, V.; Shen, J.; Evans, C.; Cooks, R. G. Collisions of Ions with Surfaces at Chemically Relevant Energies: Instrumentation and Phenomena. *Rev. Sci. Instrum.* **2001,** *72,* 3149–3179.
28. Laskin, J.; Futrell, J. H. Collisional Activation of Peptide Ions in FT-ICR Mass Spectrometry. *Mass Spectrom. Rev.* **2003,** *22,* 158–181.
29. Wysocki, V. H.; Joyce, K. E.; Jones, C. M.; Beardsley, R. L. Surface-Induced Dissociation of Small Molecules, Peptides, and Non-Covalent Protein Complexes. *J. Am. Soc. Mass Spectrom.* **2008,** *19,* 190–208.
30. Christen, W.; Even, U.; Raz, T.; Levine, R. D. Collisional Energy Loss in Cluster Surface Impact: Experimental, Model, and Simulation Studies of Some Relevant Factors. *J. Chem. Phys.* **1998,** *108,* 10262–10273.
31. Meroueh, O.; Hase, W. L. Dynamics of Energy Transfer in Peptide-Surface Collisions. *J. Am. Chem. Soc.* **2002,** *124,* 1524–1531.
32. Song, K. Y.; Meroueh, O.; Hase, W. L. Dynamics of $Cr(Co)_6^+$ Collisions with Hydrogenated Surfaces. *J. Chem. Phys.* **2003,** *118,* 2893–2902.
33. Wen, X. J.; Dagan, S.; Wysocki, V. H. Small-Molecule Analysis with Silicon-Nanoparticle-Assisted Laser Desorption/Ionization Mass Spectrometry. *Anal. Chem.* **2007,** *79,* 434–444.
34. Hua, Y.; Dagain, S.; Wickramasekara, S.; Boday, D. J.; Wysocki, V. H. Analysis of Acids with Negative Ion Silicon Nanoparticle Assisted Laser Desorption/Ionization Mass Spectrometry. In revision.
35. Dagan, S.; Hua, Y.; Boday, D. J.; Somogyi, A.; Wysocki, R. J.; Wysocki, V. H. Internal Energy Deposition with Silicon NanoParticle-Assisted Laser Desorption/Ionization (SPALDI) Mass Spectrometry. *Int. J. Mass Spectrom.* Accepted for publication.
36. Beranova, S.; Wesdemiotis, C. The Unimolecular Chemistry of Quaternary Ammonium-Ions and Their Neutral Counterparts. *Int. J. Mass Spectrom. Ion Processes* **1994,** *134,* 83–102.
37. Hudson, C. E.; Griffin, L. L.; McAdoo, D. J. CH_4 Loss from $(CH_3)_4N^+$ Revisited: How Does This High Energy Elimination Compete with CH_3? *Eur. J. Mass Spectrom.* **2004,** *10,* 767–773.
38. Steinfeld, J. I.; Francisco, J. S.; Hase, W. *Chemical Kinetics and Dynamcis*. Prentice-Hall: Englewood Cliffs, NJ, 1989.
39. Callahan, J. H.; Somogyi, A.; Wysocki, V. H. Collisions of $C_{60}^{+\cdot}$ and C_{60}^{2+} at Fluorinated and Non-Fluorinated Self-Assembled Monolayer Films. *Rapid Commun. Mass Spectrom.* **1993,** *7,* 693–699.
40. Somogyi, A.; Kane, T. E.; Ding, J. M.; Wysocki, V. H. Reactive Collisions of $C_6H_6^{-\cdot}$ and $C_6D_6^{-\cdot}$ at Self-Assembled Monolayer Films Prepared on Gold from n-Alkanethiols and a Fluorinated Alkanethiol: The Influence of Chain-Length on the Reactivity of the Films and the Neutralization of the Projectile. *J. Am. Chem. Soc.* **1993,** *115,* 5275–5283.

41. Miller, S. A.; Riederer, D. E.; Cooks, R. G.; Cho, W. R.; Lee, H. W.; Kang, H. Energy Disposal and Target Effects in Hyperthermal Collisions of Ferrocene Molecular-Ions at Surfaces. *J. Phys. Chem.* **1994,** *98,* 245–251.

42. Gu, C. G.; Wysocki, V. H.; Harada, A.; Takaya, H.; Kumadaki, I. Dissociative and Reactive Hyperthermal Ion-Surface Collisions with Langmuir-Blodgett Films Terminated by $CF_3(CH_2)_n$-, n-Perfluoroalkyl, or n-Alkyl Groups. *J. Am. Chem. Soc.* **1999,** *121,* 10554–10562.